ICAS 2016
30th Congress of the International Council of the Aeronautical Sciences
DCC, Daejeon, Korea ; September 25-30, 2016

WEIGHT REDUCTION OF CYLINDRICAL GRID STRUCTURES USING AXIAL-HELICAL-DESIGN

M. Beerhorst*, C. Hühne*
***German Aerospace Center (DLR), Braunschweig, Germany**

Keywords: *cylindrical, grid structures, compression, optimization*

Abstract

It is shown how weight reduction of cylindrical grid structures can be achieved by using axial-helical instead of helical-circumferential orientation of ribs. The optimization process mainly relies on an analytical model. A finite element model is used for validation and fine-tuning. Constraints are stability and material failure. Studies on the influence of rib heights and Young's modulus reveal potential to create lighter grids in axial helical design. Also, the main mechanical differences of both grid types and their influence on structural weight are elaborated.

1 Introduction

Cylindrical grid structures with helical and circumferential (HC) ribs are used in space engineering since several decades ([1], [2]). Mostly, their benefits regarding weight and cost were compared to the aluminum structures which they replaced. In this paper the weight optimization of axial helical (AH) grids is discussed. The general design of both grid types is shown in Fig. 1.

Closed-form analytical expressions for analysis and minimum weight of HC grids are given in [1]. A so called 'smeared stiffener' approach is used to calculate membrane and bending stiffnesses of the structures by the classical laminate theory (CLT). Good agreement between analytical model and finite element (FE) model is reported in [2] and [3].

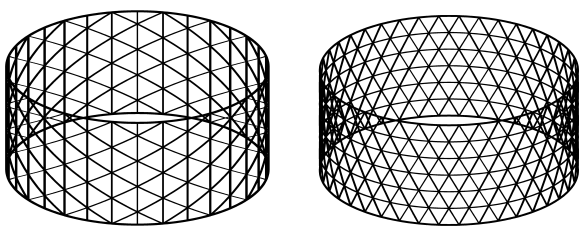

Fig. 1. Isometric view of AH (left) and HC (right) grid

In [4] a FE parameter study comparing AH and HC grids with a fixed helical angle of 45° is performed. It is stated that under stability and axial stiffness constraints a considerably lighter design is obtained for AH grids. Another FE parameter study on hexagonal HC grids under different loading conditions can be found in [5]. Similar work but considering different grid types was undertaken by [6].

Parameter studies can give an insight into the influence of the design variables. However, the true potential of structures can only be evaluated by considering optimum designs. The restriction of design variables must also be handled with care. For example, the last two mentioned papers assume the same quadratic cross sections for all rib types. The resulting designs are heavier than optimized designs with independent cross section dimensions.

The content of this paper is structured as followed: First, an analytical model of the AH grid is developed. For comparison, the analytical model of the HC grid is also shown. A short description of the FE model for validation and fine-tuning follows. After describing the optimization task in general, the weight saving potential of optimum designs is discussed for different rib heights and Young's moduli.

2 Analytical model

The spacing of ribs is assumed to be dense enough to 'smear' the ribs to form a continuous pseudo layer. Because the rib only has axial stiffness the reduced stiffness matrix in the local coordinate system is given by

$$Q_{t,11} = \delta_t E_t, \; t = \text{a, c, h.} \tag{2.1}$$

Herein t denotes the rib type (a: axial, c: circumferential, h: helical) and E the Young's modulus in longitudinal direction. The ratios of rib widths to spacings are

$$\delta_t = b_t \,/\, a_t, \tag{2.2}$$

and the relations of rib heights are

$$\beta_t = h_t \,/\, h_h. \tag{2.3}$$

Furthermore, the mass densities are related as

$$\bar{\rho}_t = \rho_t \,/\, \rho_h. \tag{2.4}$$

Processing of the pseudo layers is done according to CLT. The material law of a grid which is symmetric to the mid-surface reads

$$\begin{Bmatrix} \underline{N^0} \\ \underline{M^0} \end{Bmatrix} = \begin{bmatrix} \underline{\underline{A}} & \underline{\underline{0}} \\ \underline{\underline{0}} & \underline{\underline{D}} \end{bmatrix} \begin{Bmatrix} \underline{\varepsilon^0} \\ \underline{\kappa^0} \end{Bmatrix}. \tag{2.5}$$

The inverse of the membrane stiffness matrix is

$$\underline{\underline{\widehat{A}}} = \underline{\underline{A}}^{-1}. \tag{2.6}$$

In accordance with [7] the following non-dimensional stiffness parameters are used:

$$\varepsilon = \sqrt{\frac{\widehat{A}_{11} D_{11}}{\widehat{A}_{22} D_{22}}}, \tag{2.7}$$

$$\eta = \frac{D_{12} + 2D_{66}}{\sqrt{D_{11} D_{22}}}, \tag{2.8}$$

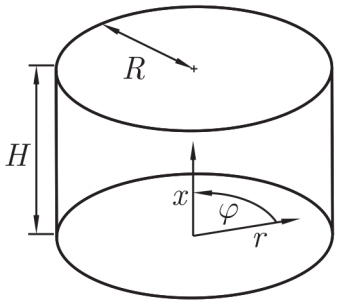

Fig. 2. Cylinder geometry and coordinate system

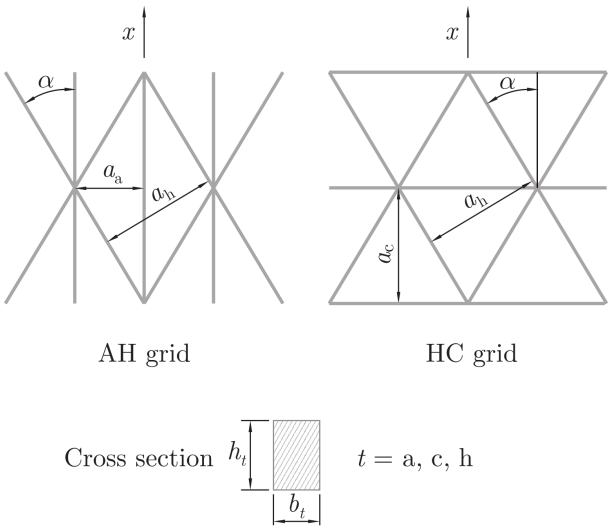

Fig. 3. Grid geometries and corresponding variables

$$\zeta = \frac{2\widehat{A}_{12} + \widehat{A}_{66}}{2\sqrt{\widehat{A}_{11}\widehat{A}_{22}}}. \tag{2.9}$$

The cylinder geometry and coordinate system are given in Fig. 2. Fig. 3 shows grid geometries and corresponding variables.

The compressive line load times the circumference yields the total force

$$P_x = 2\pi R N_x. \tag{2.10}$$

For an AH grid the stresses in the ribs are

$$\sigma_a = \frac{N_x}{h_h \beta_a \delta_a}, \; \sigma_h = 0. \tag{2.11}$$

In case of an HC grid they become

$$\sigma_c = -\frac{s^2 N_x}{h_h c^2 \beta_c \delta_c}, \sigma_h = \frac{N_x}{2c^2 h_h \delta_h}. \tag{2.12}$$

For brevity, the trigonometric functions are written as: $s = \sin(\alpha)$, $c = \cos(\alpha)$.

2.1 Failure modes

This section presents the cases of structural failure which constrain the feasible design space. Material failure of ribs occurs when

$$\sigma_{rib} = \bar{\sigma}. \tag{2.13}$$

Herein $\bar{\sigma}$ is the stress limit and σ_{rib} is σ_a in case of an AH grid and σ_h in case of an HG grid. Due to the high allowable tensile stress, failure of the circumferential ribs is not considered ([1], [8]).

Failure of the ribs by local buckling is taken into account by modeling them as Euler-Bernoulli beams:

$$\sigma_{BL} = k\frac{\pi^2 EI}{Al^2}. \qquad (2.14)$$

The factor of restraint, k, describes the boundary conditions from both ends simply supported (k = 1) to both ends fully clamped (k = 4). The bending stiffness of the rib is EI, its cross section A and the length between two rib intersections l.

It is assumed that all ribs have the same height. So the cylinder is homogeneous over the thickness. Two global buckling modes are considered: checkerboard buckling and ring buckling [7]. They are depicted in Fig. 4. In case of checkerboard buckling the buckling load is

$$P_{BC,HC} = 4\pi\sqrt{\frac{2}{3}}h^2\delta_h E_h c^2 s^2\sqrt{1+\sqrt{1+\frac{1}{2}\frac{\delta_c}{\delta_h}\frac{E_c}{E_h}\frac{1}{s^4}}} \qquad (2.15)$$

for a HC grid and

$$P_{BC,AH} = 4\pi\sqrt{\frac{2}{3}}h^2\delta_h E_h c^2 s^2\sqrt{1+\sqrt{1+\frac{1}{2}\frac{\delta_a}{\delta_h}\frac{E_a}{E_h}\frac{1}{c^4}}} \qquad (2.16)$$

for an AH grid. Ring buckling occurs at

$$P_{RG,HC} = 2\pi\sqrt{\frac{2}{3}}h^2c^2\sqrt{\delta_c\delta_h E_c E_h} \qquad (2.17)$$

and

$$P_{RG,AH} = 2\pi\sqrt{\frac{2}{3}}h^2s^2\sqrt{\delta_a\delta_h E_a E_h}, \qquad (2.18)$$

respectively.

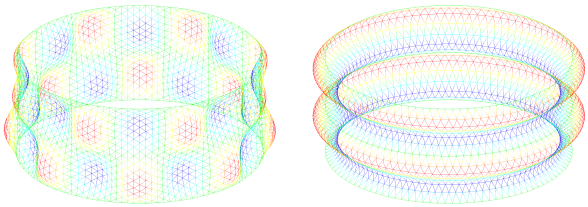

Fig. 4. Global buckling modes of cylinder: checkerboard buckling (left) and ring buckling (right)

In engineering it is common to calculate a factor of safety (FoS) by relating the allowable load or stress to the actual one:

$$n = \frac{P_{all}}{P_{act}} \geq 1 \quad \text{or} \quad n = \frac{\sigma_{all}}{\sigma_{act}} \geq 1. \qquad (2.19)$$

In the field of optimization it is more common to demand that for a valid design, constraint values are less than or equal zero:

$$g = 1 - n \leq 0. \qquad (2.20)$$

2.2 Objective function

The structural mass of an AH grid

$$m_{AH} = 2\pi RH\rho_h h_h(2\delta_h + \bar{\rho}_a\beta_a\delta_a), \qquad (2.21)$$

or a HC grid

$$m_{HC} = 2\pi RH\rho_h h_h(2\delta_h + \bar{\rho}_c\beta_c\delta_c) \qquad (2.22)$$

is the objective function to be minimized. While for the cases considered there does exist an optimum rib height for the HC grid, for the AH it would tend to infinity. Of course, this is practically only true if the assumptions of the analytical model are still valid. To generate a reasonably upper bound the height of axial ribs is expressed relatively to the optimum rib height of the HC grid by

$$\beta = \frac{h_a}{h_{\mathrm{HCOpt}}}. \qquad (2.23)$$

For all structural configurations of HC grids in this study the failure modes of local rib buckling and global ring buckling were critical. In this case the related mass is [9]

$$m^* = \frac{25\rho_h}{8}\left(\frac{72\,\bar{\rho}_c p^3}{\pi^2 k E_h^{\,2} E_c}\right)^{\frac{1}{5}}, \text{with } p = \frac{P_x}{\pi R^2}. \qquad (2.24)$$

It is obtained by dividing the mass of the cylinder by its volume:

$$m^* = \frac{m}{\pi R^2 H}. \qquad (2.25)$$

3 Finite element model

To validate the results of the analytical model a finite element model was set up. It was also used to modify the optimum result in a second stage of optimization if the validation analysis showed FoS < 1. The ribs were

modeled using two-noded quadratic beam elements (BEAM188, [10]). To accurately describe local buckling of the ribs, six elements were used between each rib intersection. Both ends of the cylinder are modeled as simply supported. All displacements at the lower end are set to zero: $u_r = u_\varphi = u_x = 0$. At the upper end u_r and u_φ are zero as well and the load is applied by a constant displacement u_x.

Widening of the ends in radial direction is normally restricted by stiff end rings. Since sizing of the end rings is also highly influenced by the type of attachment to adjacent structures it is outside the scope of this study. They are modeled as very thin beams (0.1 mm) and thus do not contribute to mass and stiffness. Because the position of circumferential ribs in a HC grid at the end of the cylinder coincides with the position of end rings, they are not included in the model. Thus the HC model has one circumferential rib less than would be obtained by a pure repetition of unit cells, making the FE model lighter by the mass of one circumferential rib compared to the analytical model. This effect is compensated when comparing masses of both models.

The analysis starts with a linear static analysis to calculate the element stresses and is followed by an eigenvalue analysis to obtain buckling loads and modes. In contrast to the analytical model which assumes constant stresses across the rib cross section the stresses can vary linearly in the FE model. This is due to the quadratic shape function of the beam elements which can capture combined axial and bending load. As a result the absolute values of the FE stresses are generally higher than the analytically determined ones.

4 Optimization process

As it was mentioned before, analytical solutions for optimum HC grid designs readily exist. Here they were adapted from [2] and [9]. The first step of optimization of AH grids was performed using the analytical model given in section 2. Design variables were rib angle α, rib height h and related widths δ_a and δ_h. To be able to construct a FE model the non-dimensional related rib widths had to be transformed into discrete ribs.

First, the distances of ribs were set to values, where the rib angle was very close to the optimum angle. While keeping the rib height of the first optimization, the rib widths were optimized using the analytical model. Since there always exist several geometric configurations with a rib angle very close to the optimum angle the changes are very small. Thus from a practical point of view this step can be omitted.

The resulting geometry values were then used for the FE validation analysis. In all cases, at least one of the FoS was below one. So the rib widths of the FE model were optimized to achieve a feasible minimum mass design. The range of the rib widths was from 80 to 130% of the initial geometry ensuring that the final design was not lying on a bound.

The open-source optimization package pyOpt was used to automatize the optimization process. Since objective function and gradients are smooth the NLPQLP algorithm [12] for smooth nonlinear programming problems was chosen. For comparison a derivative-free global constrained Augmented Lagrangian Particle Swarm Optimizer ALPSO [15] was used. This type of algorithm simultaneously searches in different areas of the design space and thus increases the chance to find the global minimum in case several minima exist. In all cases both algorithms converged to the same optimum results.

5 Influence of rib height and Young's modulus

The cylinder in the following study has a height of H = 1700 mm and a radius of R = 2000 mm. Two different sets of material properties are considered. Assuming common properties of HT fibers and a fiber volume fraction (FVF) of about 33% yields a Young's modulus of E = 80 GPa and a mass density of $\rho = 1400$ kg/m^3.

To investigate the influence of a considerable higher Young's modulus, typical IM fiber composite values and a FVF of 55 % are chosen. These lead to a Young's modulus of

150 GPa and a mass density of ρ = 1600 kg/m^3. The configurations are denoted by E08 and E15, respectively.

A conservative restraint factor of k = 1 is chosen for local rib buckling (16). Material failure is assumed at compressive stresses above $\bar{\sigma}$ = 450 MPa. To establish a comparison for a wide range of load intensities the load parameter N_x/R ranges from 0.1 to 1.0 MPa with increments of 0.1 MPa. Typical values for rockets like Ariane 6 and Proton-M lie between 0.28 and 0.45 MPa.

Optimum geometries and masses of a HC grid with E08 properties are listed in Tab. 1. For all load levels global ring buckling and local rib buckling are critical. In this case the grid angle is constant at α = 26.6°. Since all ribs have same mass densities their relative thicknesses are related by $\delta_h = 2\,\delta_c$ ([9]).

Tab. 1. Optimum values of HC-E08 grid

$\frac{N_x}{R}$/MPa	α/°	h/mm	δ_c	δ_h	$m^*/\left(\frac{\mathrm{kg}}{\mathrm{m}^3}\right)$	m/kg
0.1	26.6	13.4	0.030	0.061	2.83	60.5
0.2	26.6	17.6	0.035	0.070	4.30	91.8
0.3	26.6	20.7	0.038	0.075	5.48	117.0
0.4	26.6	23.3	0.040	0.080	6.51	139.1
0.5	26.6	25.5	0.042	0.084	7.44	159.0
0.6	26.6	27.4	0.043	0.087	8.30	177.4
0.7	26.6	29.1	0.045	0.089	9.11	194.6
0.8	26.6	30.7	0.046	0.092	9.87	210.8
0.9	26.6	32.2	0.047	0.094	10.59	226.2
1.0	26.6	33.6	0.048	0.096	11.28	241.0

The values of related masses from Tab. 1 are taken as reference to investigate the weight saving potential of different AH grid configurations. Besides the two Young's moduli mentioned earlier, different rib heights are considered. The optimum rib height of the AH grid is limited by a given upper bound. This is set to multitudes β of 1.0, 1.1 and 1.2 of the optimum rib height h_{HCOpt} of the HC-E08 grid.

Fig. 5 shows the resulting mass ratios over the load parameter. For AH grids with E08 properties the mass ratio stays nearly constant up to N_x/R = 0.7 and increases afterwards. In the constant region mass ratios are approximately 1.00, 0.96, and 0.93 for β = 1.0, 1.1, and 1.2. For selected configurations in the practically most relevant range of load parameter N_x/R, FE validation and optimization analyses were performed. Minimum FoS from FE validation

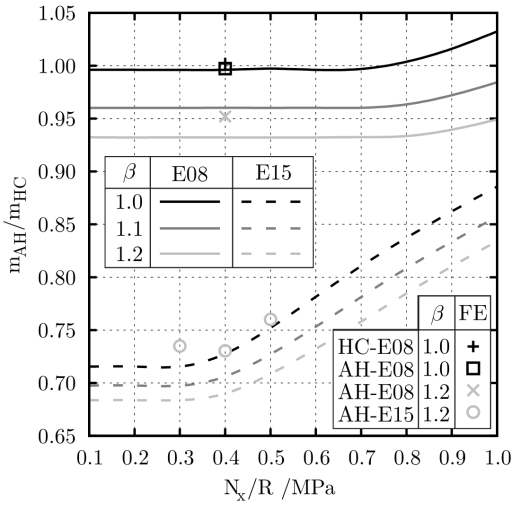

Fig. 5. Ratio of AH grid masses with E08 or E15 properties to HC-E08 grid masses. Results of optimum designs from analytical (lines) and FE model (markers).

analyses are given in Tab. 2. FoS for stability are slightly below unity in all cases and in one case also FoS for stress. Thus the agreement between the two models is very good.

In case of E15 properties the behavior of mass ratios of analytical results is similar as for E08 but the constant region ends at N_x/R = 0.3. Afterwards the increase is nearly linear. Mass ratios in the constant region for β = [1.0, 1.1, 1.2] are [0.72, 0.70, 0.68] and increase up to [0.89, 0.86, 0.83] at N_x/R = 1. The deviation of the FE to analytical results, for example 0.68 to 0.74 for N_x/R = 0.3, is higher than in case of E08 properties. The mass increase is necessary because for E15 properties the FoS from the validation analysis are lower than for E08 properties (see Tab. 3).

Tab. 2. Minimum FoS from finite element analyses using E08 material properties

$\frac{N_x}{R}$/MPa	GT	β	n_{Stab}	n_{Stress}
0.3	HC	-	0.967	1.417
	AH	1.0	0.964	1.208
		1.2	0.955	1.271
0.4	HC	-	0.988	1.296
	AH	1.0	0.974	1.069
		1.2	0.950	1.124
0.5	HC	-	0.981	1.150
	AH	1.0	0.964	0.986
		1.2	0.952	1.029

Tab. 3. Minimum FoS from finite element analyses using E15 material properties

$\frac{N_x}{R}$/MPa	β	n_{Stab}	n_{Stress}
0.3	1.0	0.922	0.913
	1.2	0.874	0.968
0.4	1.0	0.918	0.912
	1.2	0.856	0.938
0.5	1.0	0.899	0.886
	1.2	0.861	0.917

Reasons for the deviations lie in the different degree of detail of the models. In contrast to the assumptions of the analytical model, the ribs are not only loaded in constant compression but also bending. Thus the overall stresses are higher. This effect is visualized in Fig. 6. Another difference between the models is the different end support of the axial ribs. As it is shown in Fig. 6b every second rib ends in a rib intersection point. In FE analysis these ribs tend to buckle at a lower load than their neighbors whose last rib segment is shorter. The complex interaction between the ribs is also neglected by using an Euler beam in the analytical model.

These effects have a greater influence in case of E15 properties since the ribs are considerably thinner than in case of E08 properties.

6 Conclusion

The homogenized analytical modelling of cylindrical grid structures is very suitable for highly efficient structural optimization. In case of medium axial stiffness of ribs (E08) they showed very good agreement with detailed FE analyses. For axial ribs of high stiffness (E15) deviations between both analyses types increase but the influence of design variables is still described well by the analytical model. The accuracy is high enough for estimating the structural performance in the predesign phase. Also, they represent a good starting point for a second stage of optimization using more detailed FE models.

AH and HC grids have nearly same weight, when both have the optimum rib height of the

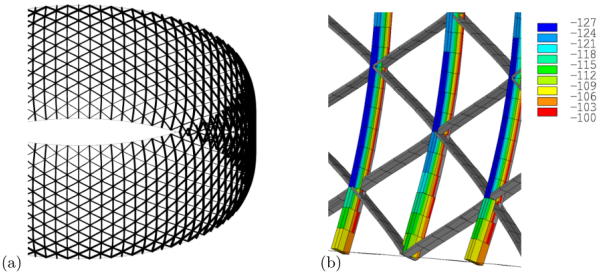

Fig. 6. Magnified deformations (a) and stresses (b)

HC grid, h_{HCOpt}. Increasing the rib height of the AH grid above h_{HCOpt} reduces weight. Increasing the Young's modulus of ribs is even more effective for reduction of mass.

References

[1] Vasiliev, V.V., Barynin, V.A., Rasin, A.F.: *Anisogrid lattice structures – survey of development and application*; Composite Structures 54, pp. 361–370, 2001.

[2] Totaro, G.: Multilevel optimization of anisogrid lattice structures for aerospace applications, Doctoral Dissertation, TU Delft, 2011.

[3] Azarov, A.V.: *Continuum and discrete models of lattice composite cylindrical shells*; Journal on Composite Mechanics and Design 18, pp. 121–130, 2012.

[4] Lohse-Busch, H.: Comparison of two carbon fiber reinforced polymer grid types with respect to stability, stiffness and mass for the use as interstage structure, in: Jerusalem, Israel, 2015.

[5] Morozov, E.V., Lopatin, A.V., Nesterov, V.A.: *Finite-element modelling and buckling analysis of anisogrid composite lattice cylindrical shells*; Composite Structures 93, pp. 308–323, 2011.

[6] Lai, C., Wang, J., Liu, C.: *Parameterized Finite Element Modeling and Buckling Analysis of Six Typical Composite Grid Cylindrical Shells*; Appl Compos Mater 21, pp. 739–758, 2014.

[7] Wiedemann, J.: *Leichtbau - Elemente und Konstruktion*, 3rd ed., Springer, Berlin et al., 2007.

[8] Vasiliev, V.V., Barynin, V.A., Razin, A.F.: *Anisogrid composite lattice structures – Development and aerospace applications*; Composite Structures 94, pp. 1117–1127, 2012.

[9] Vasiliev, V.V., Morozov, E.V.: *Advanced Mechanics of Composite Materials and Structural Elements*, 3rd ed., Elsevier, Amsterdam et al., 2013.

[10] ANSYS Inc.: *Release 15.0 Documentation for ANSYS*, Cannonsburg, Pennsylvania, U.S.A, 2013.

Contact Author Email Address

mailto: matthias.beerhorst@dlr.de

Copyright Statement